

Article

Assessment of the Operation of an SI Engine Fueled with Ammonia

Davide Lanni , Enzo Galloni , Gustavo Fontana and Gabriele D'Antuono 

Department of Civil and Mechanical Engineering, University of Cassino and Southern Latium,
03043 Cassino, Italy

* Correspondence: davide.lanni@unicas.it (D.L.); galloni@unicas.it (E.G.)

Abstract: Recently, the research interest regarding ammonia applications in energy systems has been increasing. Ammonia is an important hydrogen carrier that can also be obtained starting from renewable energy sources. Furthermore, ammonia can be used as a carbon-free fuel in combustion systems. In particular, the behavior of internal combustion engines (ICEs), fueled by ammonia, needs to be further investigated. The main disadvantage of this kind of fuel is its low laminar flame speed when it is oxidized with air. On the other hand, considering a spark-ignition (SI) engine, the absence of knock phenomena could allow a performance improvement. In this work, a 1D numerical approach was used in order to assess the performance and the operating limits of a downsized PFI SI engine fueled with pure ammonia. Furthermore, the reliability of the 1D model was verified by means of a 3D approach. Both throttled and unthrottled engine operation was investigated. In particular, different boost levels were analyzed under WOT (wide-open throttle) conditions. The potential of the 1D approach was also exploited to evaluate the effect of different geometrical compression ratio on the ammonia engine behavior. The results show that the low laminar flame speed of ammonia-air mixtures leads to increased combustion durations and optimal spark timings more advanced than the typical ones of SI engines. On the other hand, knock phenomena are always avoided. Due to the engine operating limits, the maximum rotational speed guaranteeing proper engine operation is 3000 rpm, except for at the highest boost level. At this regime, the load regulation can be critical in terms of unburned fuel emissions. Considering increased compression ratios and no boost conditions, even the 4000 rpm operating point guarantees proper engine operation.

Keywords: ammonia; carbon-free fuels; e-fuels; spark-ignition engines; downsizing



Citation: Lanni, D.; Galloni, E.; Fontana, G.; D'Antuono, G. Assessment of the Operation of an SI Engine Fueled with Ammonia. *Energies* **2022**, *15*, 8583. <https://doi.org/10.3390/en15228583>

Academic Editor: Jamie W.G. Turner

Received: 29 October 2022
Accepted: 13 November 2022
Published: 16 November 2022

Publisher's Note: MDPI stays neutral with regard to jurisdictional claims in published maps and institutional affiliations.



Copyright: © 2022 by the authors. Licensee MDPI, Basel, Switzerland. This article is an open access article distributed under the terms and conditions of the Creative Commons Attribution (CC BY) license (<https://creativecommons.org/licenses/by/4.0/>).

1. Introduction

Pollution and greenhouse gases are the main problems related to the combustion of fossil fuels in internal combustion engines (ICEs). Thus, it is crucial to find new fuels characterized by low emissions associated with the burning process. Ammonia is an important energy vector that can be used as a hydrogen carrier or as a fuel in combustion processes [1]. The energy required from the ammonia production process can be obtained via conventional processes, but also from solar or wind energy [2]. Therefore, the type of process used to produce ammonia determines the classification in brown ammonia, blue ammonia, and green ammonia [3].

The interest in ammonia as a power source started in 1878 [4] and continued during the Second World War in Belgium due to the lack of conventional fuel for heavy duty applications. Then, the use of ammonia as a fuel lost attractiveness due to its bad combustion properties. Nowadays, the interest in ammonia as an energy carrier is increasing because of having zero carbon emissions and low storage and transport costs compared to those of hydrogen. There are also some disadvantages, like low energy density, corrosive behavior, and worse combustion characteristics compared to conventional fuels. It is worth underlining that ammonia can have dangerous effects on human health, such as irritation

of the eyes and nose. Furthermore, ammonia may also be dangerous for the environment, in particular in dry, windy, and warm conditions, but its high volatility promotes dispersion in the atmosphere [1].

Table 1 summarizes the main characteristics of ammonia and compares them to those of gasoline and hydrogen. Ammonia shows clearly worse combustion characteristics with respect to gasoline. The laminar flame speed and the LHV are 87% less and 57% less than those of gasoline respectively. Nevertheless, ammonia shows a higher octane number, and therefore the knock resistance is better than that of gasoline. This allows the use of a high compression ratio in order to increase the engine efficiency and/or high boost pressure values in a supercharged engine to increase the specific power. Regarding the allowable mixture strength of ammonia–air mixtures, the flame can propagate in mixture characterized by an equivalence ratio ranging between 0.63 and 1.4 [5]; therefore, ammonia engines will be characterized by a substantially stoichiometric operation, similar to that of gasoline engines.

Table 1. Ammonia properties vs. gasoline and hydrogen properties.

	Ammonia	Gasoline	Hydrogen
Storage [1]	Liquid [300 K–11 bar]	Liquid [300 K–1 bar]	Compressed [300 K, 700 bar]
LHV [MJ/kg] [6]	18.8	44.5	120
Octane number [6,7]	130	92–98	>130
Laminar burn velocity [m/s] [6]	0.015	0.58	3.51
Auto-ignition temperature [K] [6]	924	550	858
Explosion limit [% volume ratio] [8]	16–28	1.4–7.6	4.5–75
Density [kg/m ³] [6]	0.703	740	0.082

Ammonia may be useful in ICEs [8] because it is a carbon-free fuel, it does not emit carbon dioxide, and it can be used in both spark-ignition (SI) engines and compression-ignition (CI) engines. Furthermore, the possibility of using ammonia in the marine sector is also under investigation [9,10]. ICEs could be fired using ammonia as a neat fuel [11], mixed with hydrogen [12], or in blends with conventional fuels like gasoline [13] or diesel [14,15]. In particular, hydrogen enrichment can significantly improve the combustion process of gaseous fuels in SI engines, as already shown in the work of Sun et al. [16] and Duan et al. [17].

However, the potential of pure ammonia as a fuel in internal combustion engines has been little investigated until now. As an example, Lhuillier et al. [18,19] experimentally investigated the combustion characteristics of ammonia in a modified GDI engine at 1500 rpm. They compared the combustion behavior of ammonia with hydrogen-enriched ammonia and pure methane. The results showed that ammonia can be used in an SI engine, but, in order to achieve proper engine operation, it was necessary to advance the spark timing. The efficiency was similar for each case studied, with pressure peaks lower for ammonia compared to those of other fuels. Mounaim-Rousselle et al. [20] focused their attention on the operating limits of a small GDI engine modified to run with premixed ammonia–hydrogen–air mixtures (hydrogen content ranging from 0 to 10% by volume). Keeping the original spark plug device, they analyzed engine cycle variation and exhaust gas emissions when varying the intake air pressure (from about 0.55 bar up to 1 bar) at different engine speeds (from idle speed to 2000 rpm) for lean, stoichiometric and rich air–fuel mixtures. Running with pure ammonia, they found the engine could stably operate at up to 1500 rpm when the intake air pressure was equal to 1 bar, while the engine cycle variation limited low load operation. In particular, they indicated a coefficient of variation of IMEP higher than 5% when the intake air pressure was less than 0.75 bar. The engine was not able to operate at 2000 rpm for any of the air intake pressures. When the hydrogen percentage in the fuel mixture was 10%, the authors achieved proper engine operation for all considered cases.

In [21], the authors investigated the combustion of lean gasoline–ammonia–air mixtures in an SI engine derived from a CI engine characterized by a glow plug and a sub-

chamber. They found that increasing the ammonia concentration reduces the pressure peak, while NO_x increases. The influence of the glow plug on IMEP and thermal efficiency was negligible in almost all conditions.

El Fattah et al. [22] focused on the exhaust emissions and performance of an SI engine fueled with water–ammonia–gasoline blends. They found that when adding water–ammonia to gasoline, the engine thermal efficiency increased, but the CO formation also increased due to the occurrence of incomplete combustion. Additionally, NO_x emissions increased with the volume percentage of the water–ammonia solution.

In [23] Sahin et al. investigated the behavior of a small dual fuel CI engine running with premixed water–ammonia solutions. The addition of ammonia determined an increase in engine efficiency at all the investigated speed and load values. Even in this case, they found an increase in NO_x related to the nitrogen present in NH_3 . The authors also pointed the attention on the damages of some elements of the carburetor used to add the fuel.

A literature review shows that fueling ICEs with pure ammonia leads to increased combustion durations, which could limit the operation of light-duty engines. The aim of this work is to explore the operating limits of a light-duty turbocharged SI engine fueled with pure ammonia considering different engine speeds, boost pressure levels and throttle openings. In particular, the behavior of a small ammonia engine is investigated by means of a numerical approach able to reproduce the whole engine layout. This approach also allows investigating the influence of increased geometrical compression ratios on both the performances and the operating range of the engine.

2. Materials and Methods

To investigate the potential of ammonia as a fuel for internal combustion engines, the conversion of a typical downsized gasoline engine, developed for light duty vehicles, was considered (Section 2.1). The performance of the converted engine was estimated by means of a 1D model developed to reproduce the engine operation when the fuel is varied (Section 2.2). The reliability of 1D results mainly depends on a proper prediction of the in-cylinder pressure development. Thus, 3D calculations were also considered in order to model the flame propagation within the combustion chamber of the ammonia engine (Section 2.3). The comparison between 1D and 3D results, with respect to some operating points, gives an idea of the reliability of both of the calculation models.

2.1. The Engine

The engine analyzed in this work is a typical port fuel injection (PFI) turbocharged SI engine for automotive use. It was developed to run with straight regular grade gasoline fueling. Its main characteristics are shown in Table 2.

Table 2. Engine main characteristics.

Model	4 Cylinders, 4 Valves/cyl
Displacement [cm^3]	1368
Bore/Stroke/Con. Rod [mm]	72/84/129
Compression Ratio [-]	9.8
Combustion Chamber Shape	Pent Roof
Max Power (ISO Conditions) [kW]	110 @ 5500 rpm
Max Torque (ISO Conditions) [Nm]	230 @ 3000 rpm
Turbocharger group	IHI RHF3

2.2. 1D Numerical Approach

A 1D approach was used to assess the operation of the engine running with ammonia. The model reproduces the whole engine layout (Figure 1) in order to perform full engine cycle simulations. It was described in detail in [24,25]. Briefly, in-pipe flow was estimated using a finite volume approach, while the turbocharger was modeled using the steady flow maps provided by the manufacturer. To allow boost pressure control, a part of the

exhaust gas can bypass the turbine simulating the wastegate valve operation. The heat transfer rate through the walls of the combustion chamber was estimated by means of the well-known Woshni correlation, while the friction losses were calculated as a function of the engine speed.

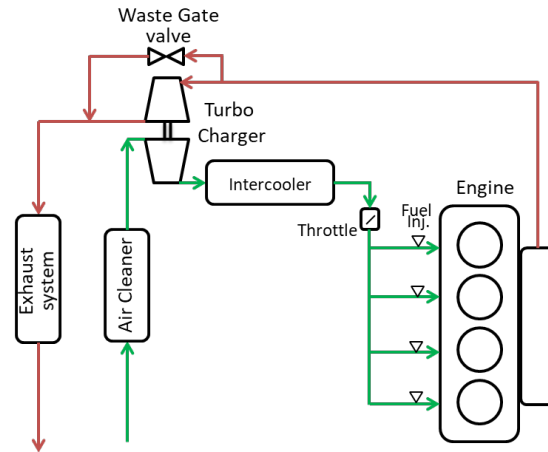


Figure 1. Schematic layout of the engine [25].

Ammonia oxidizes according to Equation (1). The dissociation of the combustion products is not considered, so the ammonia molecules can be oxidized completely or not depending on the charge conditions.



The model used predicts the burning rate for homogeneous charge spark-ignition engines based on the work of Keck and Tabaczynski [26,27]. This approach takes into account the cylinder geometry, the spark location and timing, the air motion and the fuel properties. The calculated turbulent flame speed depends on both laminar flame speed and turbulent flow indices according to an entrainment model. A spherical flame propagates from the sparkplug, while a turbulent entrainment process controls the combustion rate, as shown in Equations (2) and (3).

$$\frac{dM_e}{dt} = \rho_e A_f (u' + S_L) \quad (2)$$

$$\frac{dM_b}{dt} = \frac{(M_e - M_b)}{\tau} \quad (3)$$

where M_e is the mass of the fresh gas mixture entering the flame front and M_b is the burned mass. A_f is the surface area at the edge of the flame front, ρ_e is the fresh gas density, u' is the turbulent intensity and S_L is the laminar flame speed. τ is a time constant depending on the ratio between the Taylor microscale of turbulence and the laminar flame speed. The Taylor scale is calculated as a function of the integral length of turbulence and the kinematic viscosity of the unburned mixture. Following the hierarchical approach described in [28], the mean turbulent length scale and the mean turbulent intensity were imposed, exploiting the flow field details provided by 3D calculations.

The knock occurrence was predicted taking into account the empirical induction time (τ_{id}) of the air–fuel mixture. It was assumed that knock occurs when $\int_0^t dt / \tau_{id}(t) = 1$ [29]. When knock occurs, the knock intensity is estimated as in Equation (4) [30].

$$KI = (1 - x_b)(cr - 1) \sqrt{1 - \frac{\theta_k}{\theta_{ref}} \frac{N}{N_{ref}}} \quad (4)$$

where x_b is the mass of burned fuel, cr is the compression ratio, θ_k is the knock onset crank angle, and N the engine speed, θ_{ref} the maximum crank angle for which knock is still audible and is set to 50 CAD. N_{ref} is a tuning parameter set equal to 3500 rpm. As in [24] and [25], it was assumed that tolerable knock corresponds to a KI level less than or equal to 0.5.

The model was previously validated considering the engine running with pure gasoline both at full and partial load [24]. Furthermore, it correctly reproduced the behavior of the engine running with different alcohol–gasoline blends [31] and was also used to predict the performance of the same engine in case of hydrogen fueling [25]. This encouraged the authors to use the model also to predict the behavior of the analyzed engine running with pure ammonia. Of course, the thermochemical properties of ammonia–air mixture were considered, while the laminar flame speed was calculated using the correlations proposed by Goldmann and Dinkelacker [32]:

$$S_L = S_{L0} \left(\frac{T_u}{T_0} \right)^\alpha \left(\frac{p}{p_0} \right)^\beta k \quad (5)$$

$$S_{L,0} = (a_1 + b_1\lambda) / (1 + c_1\lambda + d_1\lambda^2) \quad (6)$$

$$\alpha = a_2 + b_2\lambda + c_2\lambda^2 + d_2\lambda^3 + e_2\lambda^4 + f_2\lambda^5 \quad (7)$$

$$\beta = a_3 + b_3\lambda + c_3\lambda^2 + d_3\lambda^3 + e_3\lambda^4 + f_3\lambda^5 \quad (8)$$

$$k = \begin{cases} k_1 k_2 \frac{p}{p_0} \left(\frac{p}{p_0} \right)^{k_3} \lambda^{k_4} & \forall T_u \leq T_0 \wedge p \leq 0.5 \text{ MPa} \\ 1.0 & \forall T_u > T_0 \wedge p > 0.5 \text{ MPa} \end{cases} \quad (9)$$

where T_u and p are the temperature and pressure of the unburned mixture, respectively. T_0 and p_0 are the reference conditions of temperature and pressure equal to 300 K and 0.1 MPa, respectively. λ is the air–fuel equivalence ratio and is equal to $1/\phi$. Coefficients a , b , c , d , e , f and k are tabulated as a function of pressure and temperature ranges [32].

Figure 2 shows the laminar flame speed at ambient condition for ammonia–air mixtures calculated by the relationships mentioned above and compares them with those calculated for gasoline–air mixtures according to [33]. As expected, gasoline shows a faster laminar flame speed. Both ammonia and gasoline exhibit a peak at an equivalence ratio of 1.1. Considering stoichiometric conditions for both mixtures, the laminar flame speed for ammonia is 0.06 m/s, approximately 82% less than that of gasoline.

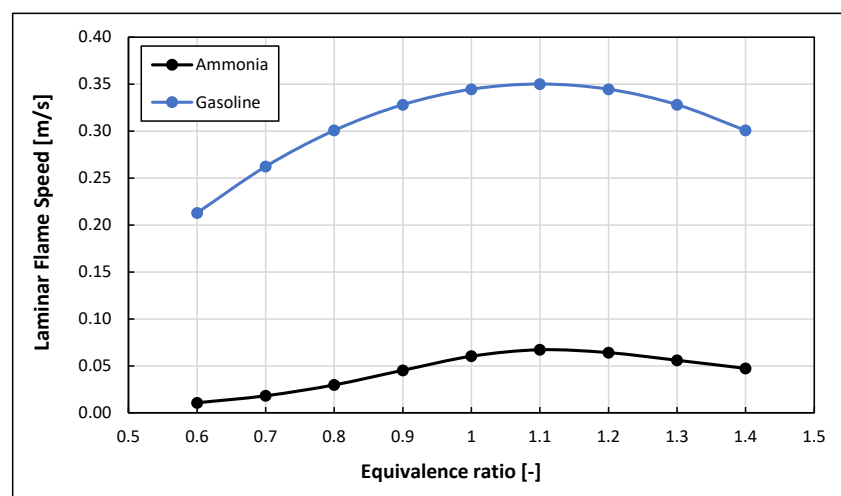


Figure 2. Laminar flame speed under ambient conditions calculated for gasoline–air mixtures and ammonia–air mixtures.

The induction time of the ammonia–air mixture is calculated by means of Equation (10) [34]:

$$\tau_{id} = Ap^n \cdot e^{\frac{E_a}{RT}} \quad (10)$$

where A is equal to 0.0658 ms, n is equal to -0.779 , E_a represents the global activation energy and is equal to 35.574 kcal/mol, and R is the universal gas constant.

2.3. 3D Numerical Approach

A 3D computational model was used to reproduce some of the operating points investigated by means of the 1D model. The model was built using the commercial code AVL Fire. The partial differential transport equations were discretized on the basis of a finite volume method. A first-order (Euler) implicit differencing scheme was used for time discretization. Second-order schemes were used for continuity and momentum equations. An upwind scheme was used for turbulence and energy equations. Turbulent effects were described by means of the standard k - ϵ approach. The ammonia oxidation process was simulated implementing the chemical-kinetics mechanism proposed by Nakamura et al. [35] within the 3D model. This mechanism consists of 33 species and 232 reactions.

Due to the symmetry of the engine geometry, only half of the fluid domain was modeled. The combustion chamber, the intake valve, and the intake port were discretized by means of polyhedral elements in order to obtain a dynamic unstructured grid (Figure 3) which reproduced the intake stroke, the compression stroke and the following expansion stroke of the engine. The minimum number of cells in the grid is about 50,000 (firing TDC), while the maximum number is about 350,000 (BDC during the intake stroke). Boundary and initial conditions were set by means of calculations carried out using the 1D model described above.

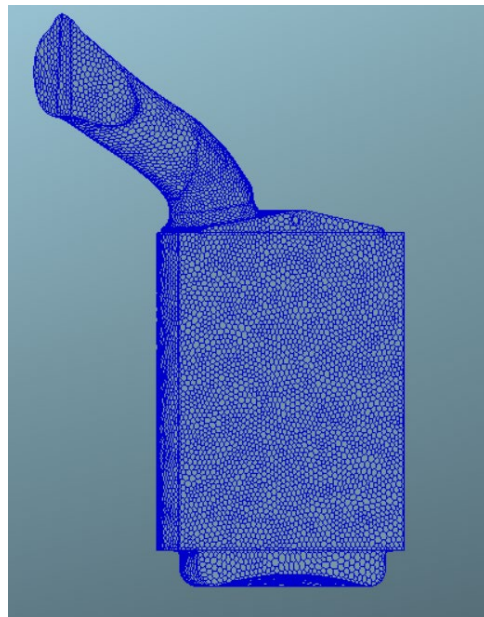


Figure 3. Engine grid.

3. Results

To assess the behavior of the analyzed engine with ammonia fueling, steady-state engine operating points were investigated. In each case, wide open throttle (WOT) operation was imposed, except for the analysis referring to the effect of throttling on engine performance. First, 3D calculations were carried out to reproduce some operating points and to compare the 3D results with those obtained from the 1D calculations. Then, several analyses were performed using the 1D approach in order to assess both the performance

and the operating limits of the ammonia engine. In the following sub-sections, the results of each analysis are described in detail.

3.1. Comparison between 3D and 1D Results

The engine operating points shown in Table 3 were simulated using both 3D and 1D approaches. No boost indicates fully open wastegate valve conditions. In particular, the optimal spark timing for maximum torque was identified by means of 1D calculations. The same operating point was reproduced using the 3D approach. It is worth highlighting that spark timings more advanced than typical ones of SI engines are needed to obtain a proper combustion with ammonia fueling due to its low laminar flame speed. This is confirmed by the results of the experimental analysis carried out in [18]. Naturally, the more the engine speed increases, the more the optimal spark timing will advance (Table 3).

Table 3. Test cases, WOT, no boost. Optimal spark timing.

Engine Speed [rpm]	2000	3000
Spark advance [$^{\circ}$ bTDC]	82.9	102.1
Equivalence ratio [-]	1	1

Figure 4 shows the in-cylinder pressure evolution and the heat release rate predicted by both 3D and 1D models. The good agreement between the results of both approaches further encouraged the authors to use the 1D approach to perform an analysis of both the performance and the operating limits of the ammonia engine. Furthermore, the calculated burned fuel fraction at the exhaust valve opening (EVO) is shown in Table 4. The 1D model overestimates the amount of unburned ammonia because it does not take into account the partial oxidation of ammonia. The result is an underestimation in terms of burned fuel fraction less than 2%.

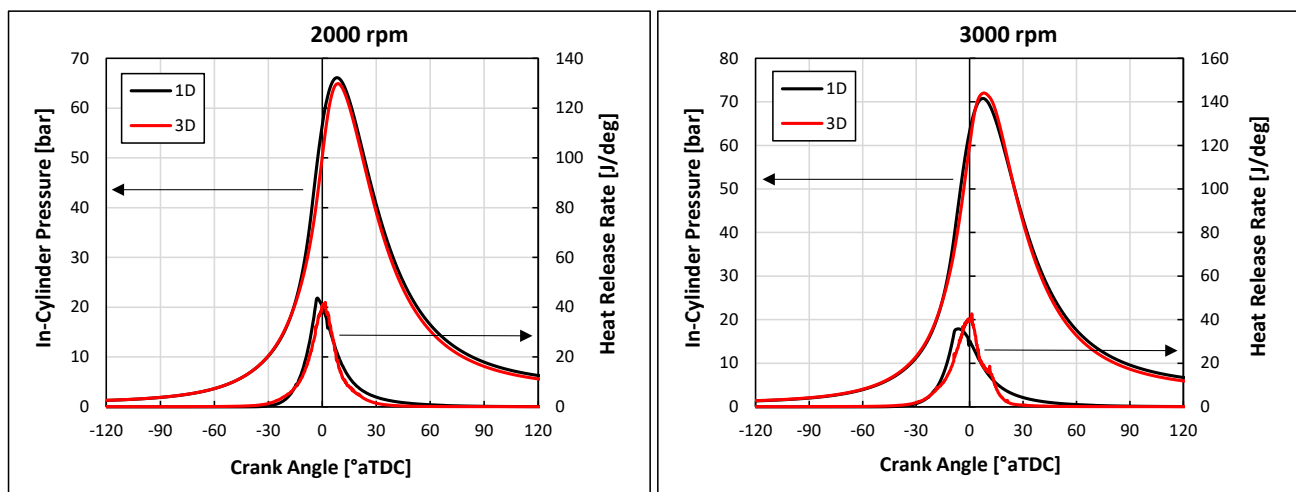


Figure 4. In-cylinder pressure and heat release rate for both 2000 and 3000 rpm operating points, WOT. Comparison between 1D and 3D results. $\phi = 1$, no boost.

Table 4. Burned fuel fraction at EVO calculated by both 3D and 1D model. WOT, no boost, optimal spark timing.

Engine Speed [rpm]	2000		3000	
	3D	1D	3D	1D
Burned fuel fraction at EVO [%]	99.95	98.84	99.99	98.42

3.2. Engine Performance and Operating Limits

First, parametric analyses of the effects of both spark timing and equivalence ratio on engine performance and combustion development were performed at 1500 rpm. Then, in subsequent analyses, the spark angle was set for maximum torque and stoichiometric combustion was imposed. Throttled and unthrottled engine operating points were analyzed. In particular, WOT operation was investigated both for increasing boost pressures (BP) and increasing geometrical compression ratio.

Analyses have been carried out taking into account the engine operating limits reported in Table 5. Unfortunately, the 1D model is not able to predict the cycle-to-cycle variation. Thus, this important constraint was not considered.

Table 5. Engine operating limits.

Peak pressure [bar]	≤ 100
Exhaust gas temperature [K]	≤ 1173
Spark advance [$^{\circ}$ bTDC]	≤ 110
Knock intensity [-]	≤ 0.5

It is worth underlining that no knocking condition was detected in any of the analyzed cases.

Finally, it was considered that unburned ammonia cannot be released through the engine exhaust. As shown in Table 4, the 1D model overestimates the amount of unburned ammonia calculated in the various cases. For this reason, in the subsequent analysis a fuel burned mass fraction equal to 98% was considered as the minimum acceptable value.

3.2.1. Effect of Spark Timing

The effect of different spark advances (SA) on engine performance and combustion characteristics was evaluated at 1500 rpm setting the equivalence ratio equal to 1 and no boost WOT conditions. The results are shown in Figure 5 and Table 6. Advanced spark timings lead to an increase in combustion delay (CA0-2) and a reduction of combustion duration (CA10-90), as reported in Table 6. The CA10-90 reduction prevails over the CA0-2 increase. Thus, when the spark advance increases, both the pressure peak (Figure 5, left) and the burned fuel fraction (Table 6) at EVO increases. The spark advance value which maximizes both engine power (Figure 5, right) and efficiency (Table 6) is 69° bTDC. Setting the latter value, the brake specific fuel consumption (BSFC) is about 420 g/kWh (Table 6).

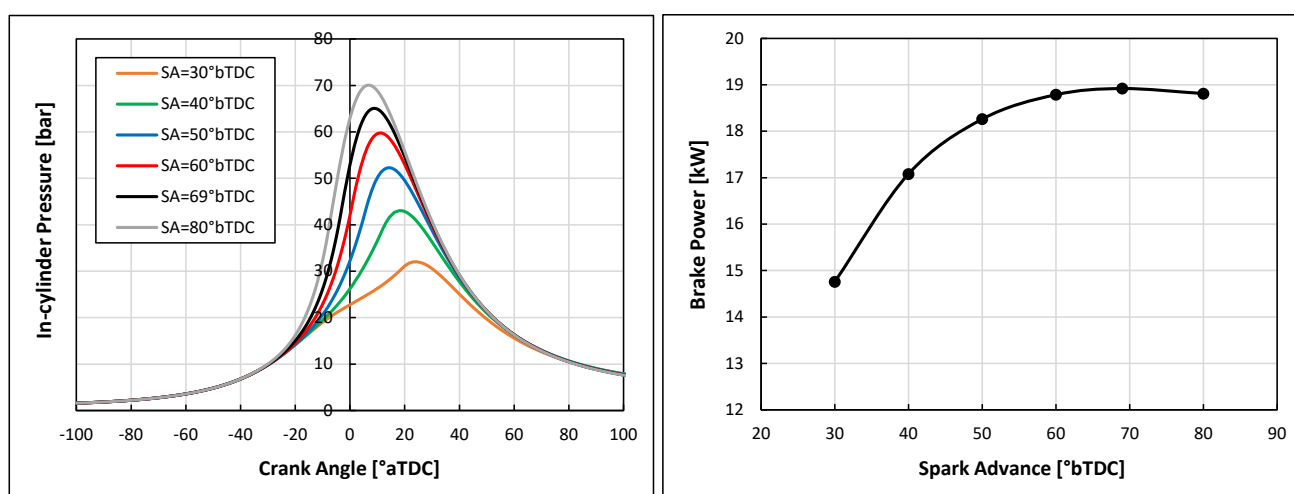


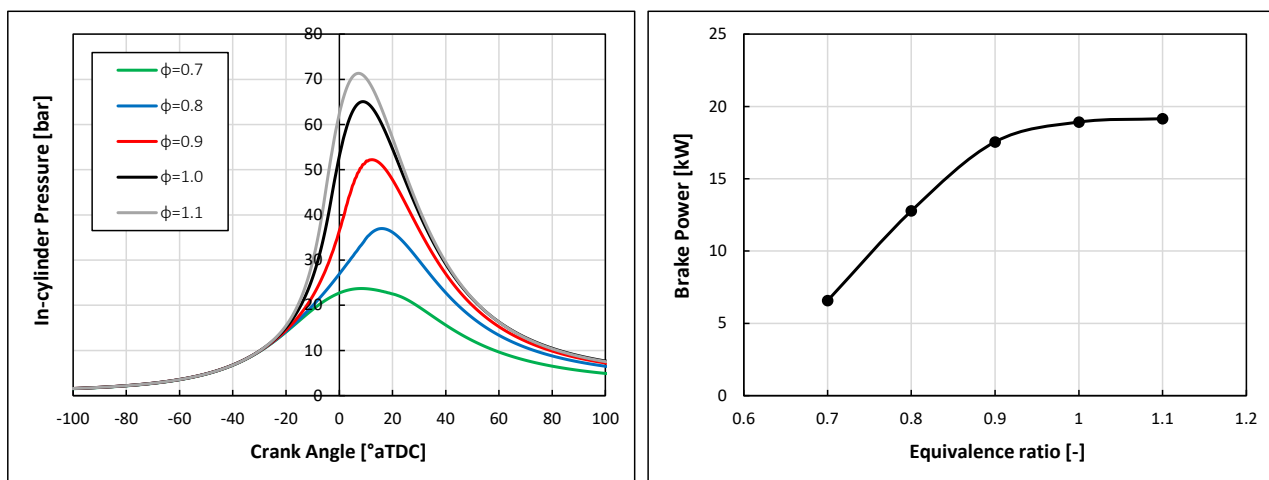
Figure 5. In-cylinder pressure (left) and brake power (right) for different spark advances; 1500 rpm, $\phi = 1$. WOT, no boost.

Table 6. Combustion characteristics and engine performance; 1500 rpm, $\phi = 1$, WOT, no boost.

Spark Advance [$^{\circ}$ bTDC]	30	40	50	60	69	80
CA0-2 [CAD]	29.3	33.3	38.5	44.2	49.7	56.5
CA10-90 [CAD]	101.9	50.1	35.8	30.5	28.1	26.8
Burned Fuel Fraction at EVO [%]	91.3	95.7	97.7	98.6	99.1	99.4
Brake Efficiency [%]	29.7	34.4	36.8	37.9	38.2	38.0
BSFC [g/kWh]	539.9	465.8	435.1	422.6	419.5	421.7

3.2.2. Effect of Equivalence Ratio

The effect of the mixture composition was investigated under 1500 rpm, wide open throttle, no boost conditions. The spark advance was set to be equal to 69° bTDC, i.e., the optimal spark advance under stoichiometric conditions for $\phi = 1$. Figure 6 and Table 7 show the obtained results. Both combustion delay and combustion duration decrease for increasing values of the equivalence ratio leading to higher values of the burned fuel fraction at EVO (Table 7). In particular, the maximum mass fraction burnt (99.1%) is obtained for the stoichiometric mixture, while for $\phi < 0.9$ the 90% mass fraction burnt is not reached. As a result, of the faster combustion, the peak pressure increases for increasing values of the equivalence ratio (Figure 6, left) leading to higher engine power (Figure 6, right). The maximum engine efficiency and the minimum BSFC are reached for $\phi = 0.9$, but the overall combustion duration is higher with respect to stoichiometric conditions (Table 7). For this reason, in the following analyses, stoichiometric combustion was imposed in order to obtain a good compromise between engine efficiency and combustion duration. This choice was made since, at higher engine speeds, a too slow combustion could not allow a proper engine operation. On the other hand, rich mixtures were avoided since they lead to ammonia emissions which are not acceptable from an environmental point of view.

**Figure 6.** In-cylinder pressure (left) and brake power (right) for different equivalence ratios; 1500 rpm, SA = 69° bTDC, WOT, no boost.**Table 7.** Combustion characteristics and engine performance; 1500 rpm, SA = 69° bTDC, WOT, no boost.

Equivalence Ratio [-]	0.7	0.8	0.9	1.0	1.1
CA0-2 [CAD]	66.3	59.3	53.9	49.7	47.7
CA10-90 [CAD]	/	/	41.2	28.1	24.6
Burned Fuel Fraction at EVO [%]	61.7	87.4	96.5	99.1	91.0
Brake Efficiency [%]	18.0	31.1	38.6	38.2	35.9
BSFC [g/kWh]	889	516	415	420	446

3.2.3. Effect of Boost Pressure

The performances of the ammonia engine were investigated by varying the engine speed and considering different boost levels (Figures 7–10). In each operating point, the mixture was set to be stoichiometric and the spark angle was adjusted to the optimal value complying with the limit $SA \leq 110^\circ$ bTDC.

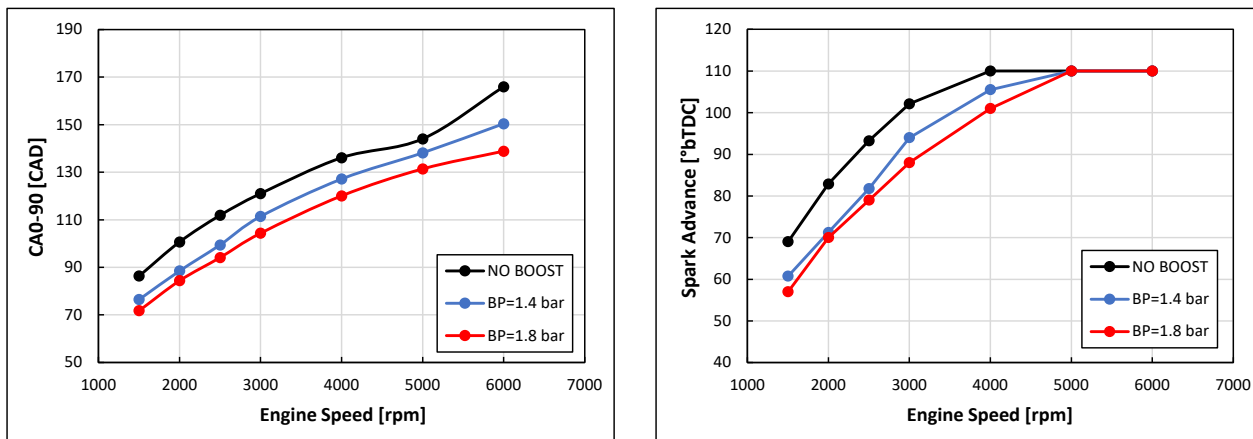


Figure 7. Combustion duration (0–90%) (left) and optimal spark advance (right) for different boost levels. $\phi = 1$. WOT.

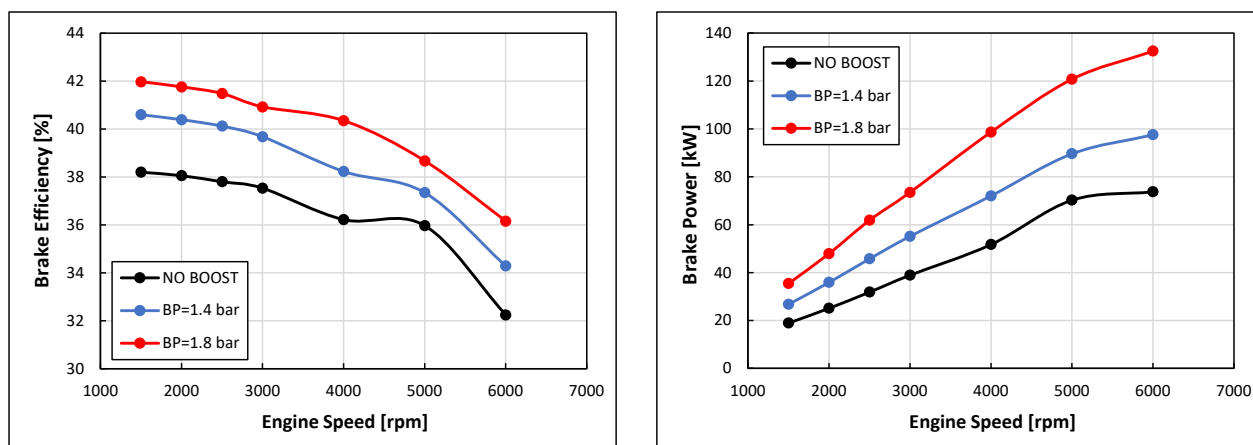


Figure 8. Brake efficiency (left) and brake power (right) for different boost levels. $\phi = 1$. WOT.

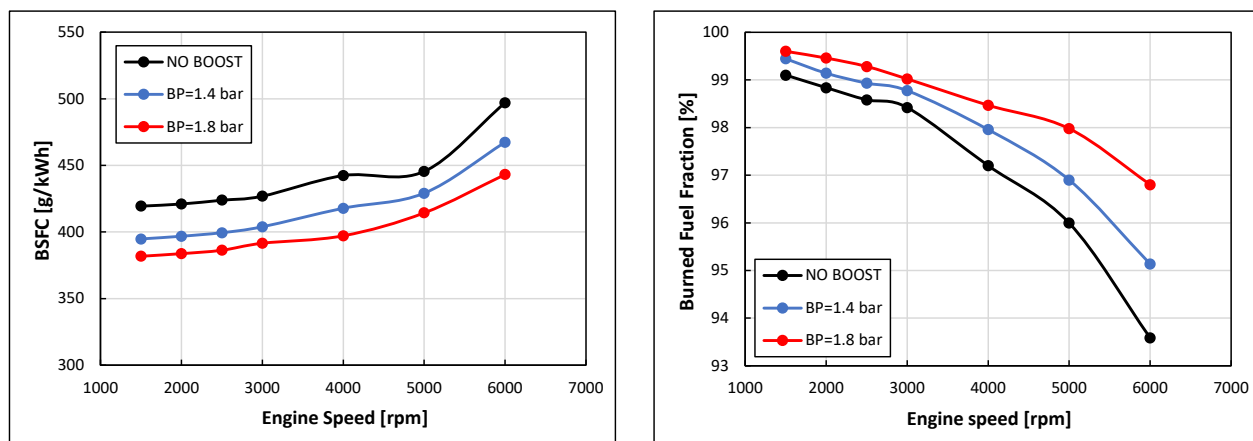


Figure 9. BSFC (left) and burned fuel fraction (right) for different boost levels. $\phi = 1$. WOT.

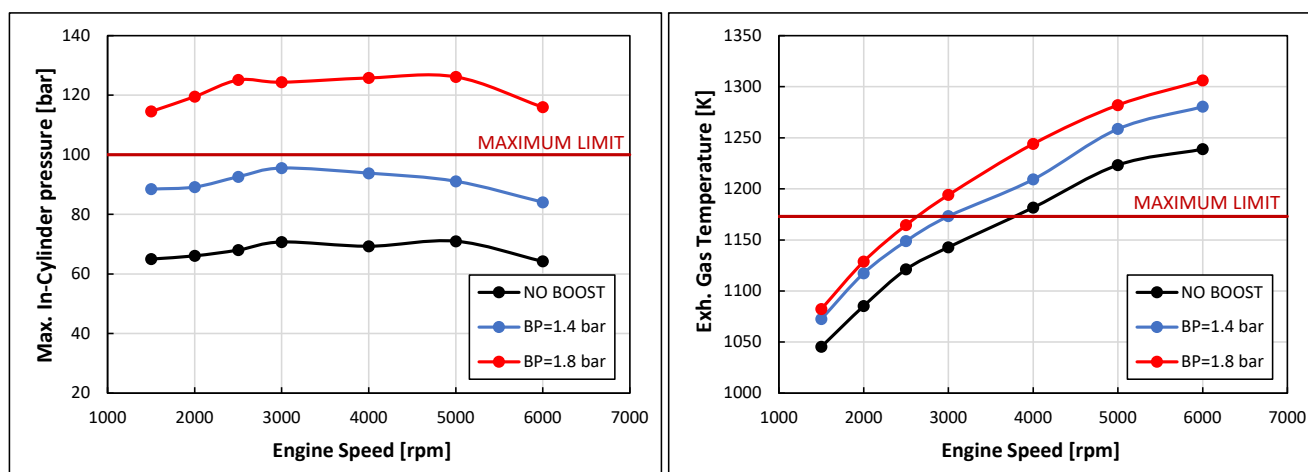


Figure 10. Maximum in-cylinder pressure (left) and exhaust gas temperature (right) for different boost levels. $\phi = 1$. WOT.

Results related to engine speeds ranging from 1500 rpm to 6000 rpm are shown. The combustion duration increases with increasing engine speed, while it decreases with increasing boost pressure (Figure 7, left). The optimal spark advance consequently varies, reaching the imposed constraint at the highest engine speeds (Figure 7, right). It is worth underlining that the increase in the angular combustion duration (CA0-90) with increasing engine speed is typical of SI engines, but it can be critical in the case of ammonia fueling due to the low laminar flame speed of ammonia–air mixtures (Figure 2). At medium and high rotation speeds, the engine could not properly operate [20]. Combustion durations comparable to those obtained in this work were experimentally measured in [18].

The engine efficiency grows with the boost pressure (Figure 8, left) showing very high values at low engine speeds (from 38% to 42% at 1500 rpm). It decreases when the engine speed increases because the combustion slows down. However, the engine efficiency always remains over 32%. The BSFC consequently varies from a minimum value of about 380 g/kWh to a maximum value of about 500 g/kWh (Figure 9, left). The engine power also reaches very interesting values (Figure 8, right), like those of gasoline engines. At 6000 rpm, with a boost pressure equal to 1.4, the engine can deliver about 100 kW.

Unfortunately, higher engine speeds appear unsustainable considering the trends of both the unburned ammonia content and the temperature of the exhaust gas leaving the cylinders. Indeed, increasing combustion durations lead to an incomplete fuel combustion (Figure 9, right) and to higher temperatures of the exhaust gases which leave the cylinders (Figure 10, right). It is worth noting that when increasing the boost level, the burned ammonia fuel fraction improves, while the exhaust gas temperature increases at a given engine speed.

In the end, the maximum allowable engine speed is about 3000 rpm both at no boost operation (due to the unburned fuel constraint) and at BP = 1.4 bar (due to the exhaust gas temperature constraint). The boost level 1.8 is unacceptable, since the maximum in-cylinder pressure exceeds the maximum allowable value in each operating point (Figure 10, left).

3.2.4. Effect of Compression Ratio

The effects of increasing geometrical compression ratios (from 9.8 to 11.0) on the engine behavior were evaluated at wide throttle operation, no boost condition. As in the previous analysis, the spark angle was adjusted to the optimal value complying with the limit $SA \leq 110^\circ \text{BTDC}$.

For each engine speed, the increase in the compression ratio leads to a reduction in the combustion duration and to a consequent decrease in the optimal spark advance (Figure 11). This is due to the higher pressure in the cylinder during the compression

stroke, which increases the charge temperature and, consequently, the flame speed. The favorable thermodynamic effect due to both the increase in the compression ratio and the faster combustion determines a not negligible improvement in the engine efficiency and a slight increase in the engine power (Figure 12).

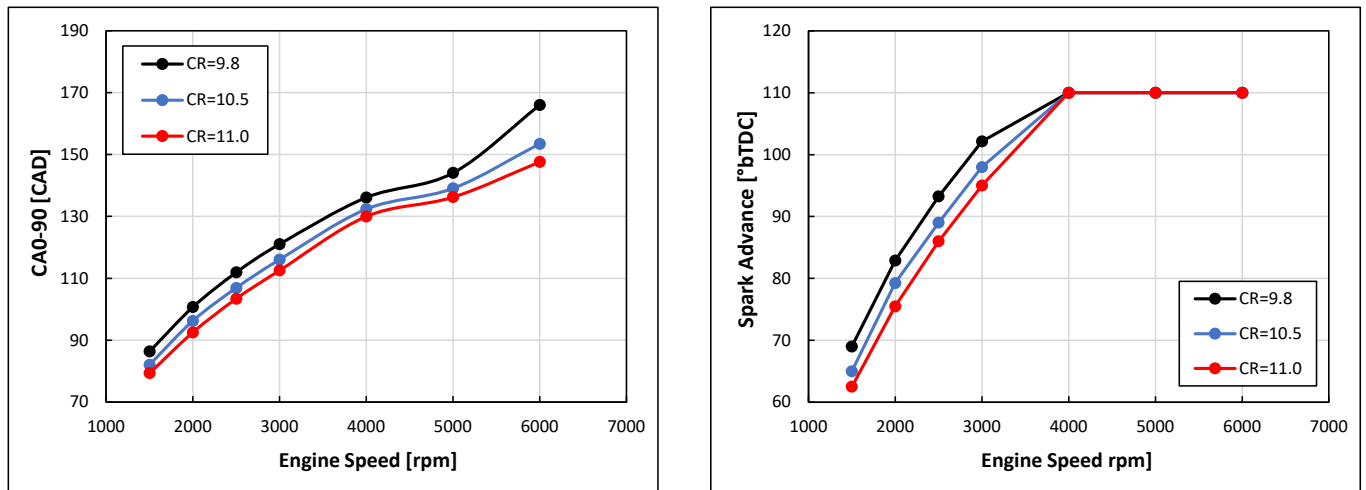


Figure 11. Combustion duration (left) and optimal spark advance (right) for different compression ratios. $\phi = 1$, WOT, no boost.

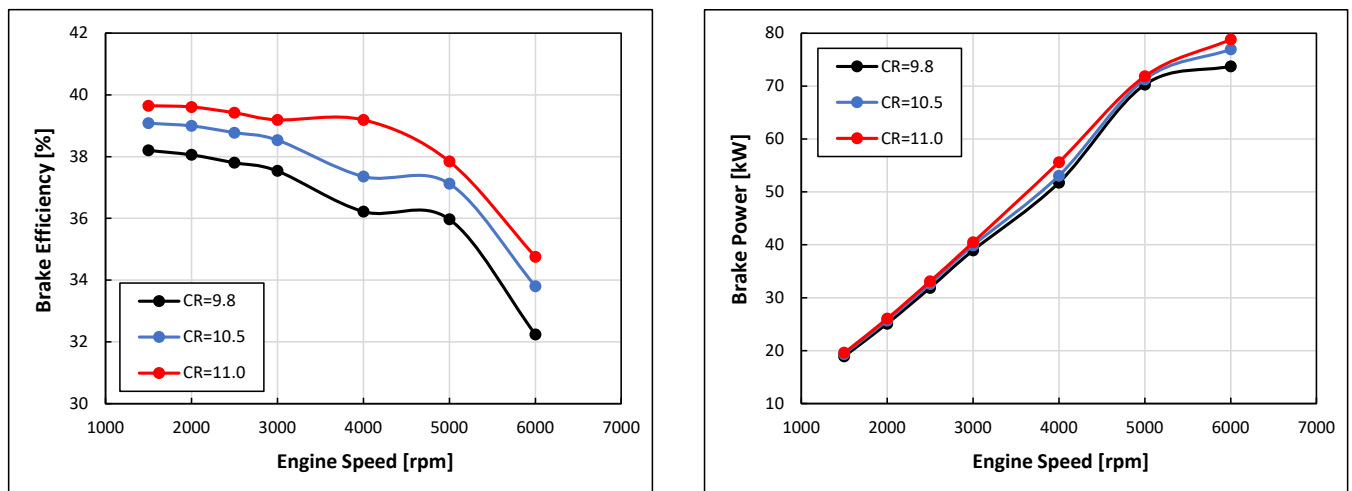


Figure 12. Brake efficiency (left) and brake power (right) for different compression ratios. $\phi = 1$, WOT, no boost.

Higher geometrical compression ratios are beneficial for both the quantity of unburned fuel at EVO (Figure 13, right) and the exhaust gas temperature (Figure 14, right). Indeed, faster combustion makes the combustion process more complete. Furthermore, the temperature of the exhaust gas leaving the cylinder decreases due to the increased effective expansion phase. On the other hand, the peak pressures increase while remaining below the maximum limit (Figure 14, left). At the end, for no boost conditions, with increased compression ratios, even the 4000 rpm operating point complies with the operating limits, guaranteeing proper engine operation.

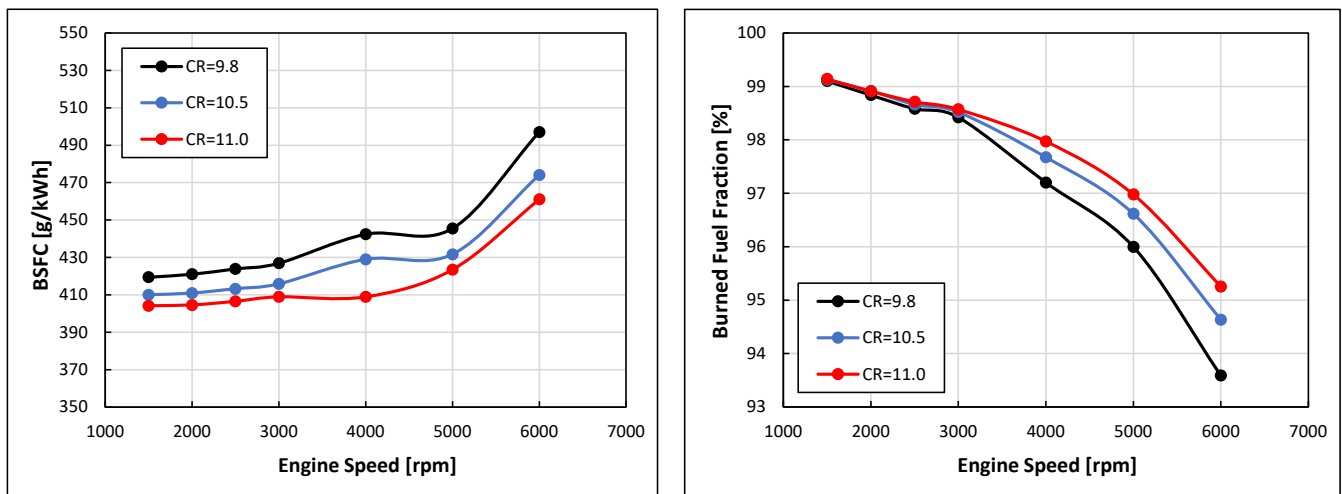


Figure 13. BSFC (left) and burned fuel fraction (right) for different compression ratios. $\phi = 1$, WOT, no boost.

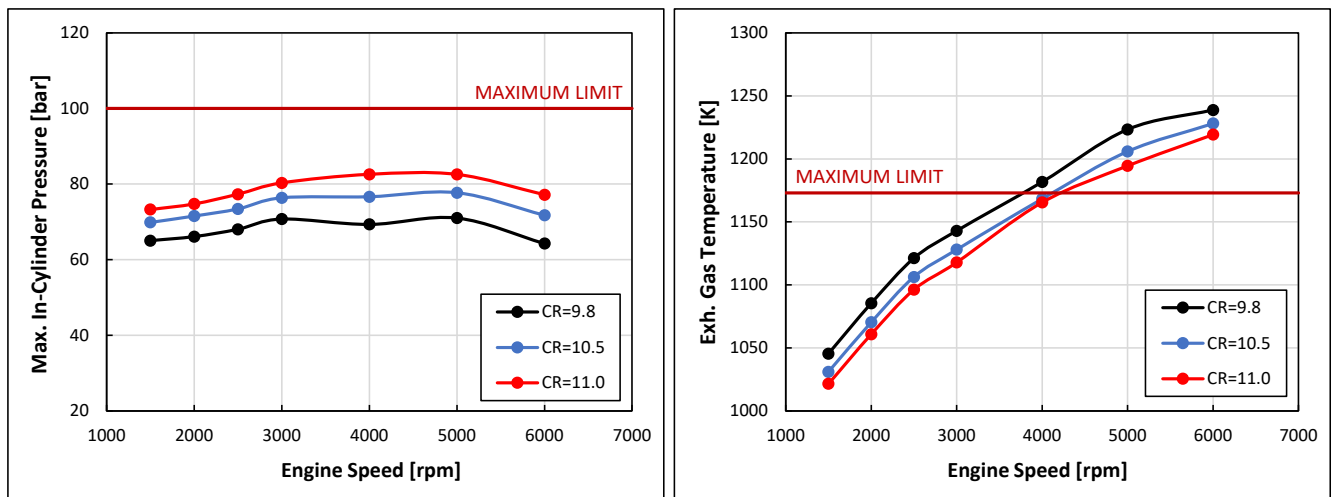


Figure 14. Maximum in-cylinder pressure (left) and exhaust gas temperature (right) for different compression ratios. $\phi = 1$, WOT, no boost.

3.2.5. Effect of Throttle Opening

Considering no boost conditions, stoichiometric air–ammonia mixture and optimal spark timing, the effect of different throttle openings on engine behavior was evaluated. The analysis was carried out at 1500 and 3000 rpm operating points. The load regulation curves are shown in Figure 15. As is typical in PFI SI engines, when throttling the engine, the brake efficiency decreases due to the growing of the pumping losses. Furthermore, the combustion duration increases due to the higher dilution of the charge (Figure 16, left) which reduces the laminar flame speed Equations (3)–(7). Higher CA₀₋₉₀ values at decreasing engine loads lead to a reduction of the burned fuel fraction which is amplified for the highest engine speed (Figure 16, right). These results clearly show that, at 3000 rpm, the load regulation can be critical in terms of unburned fuel emissions. It is worth noting that using a numerical approach it has not been possible to evaluate the engine cycle variation. Thus, the operating range could be further reduced due to an excessive value of the coefficient of variation of IMEP [20].

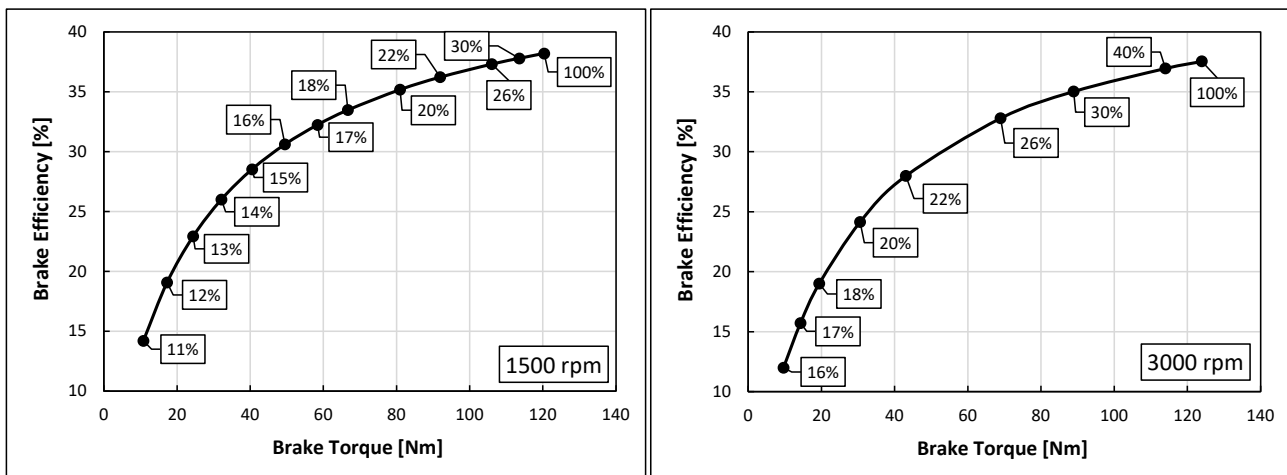


Figure 15. Brake efficiency as a function of the brake torque. The labels highlight the different throttle opening values. $\phi = 1$, no boost.

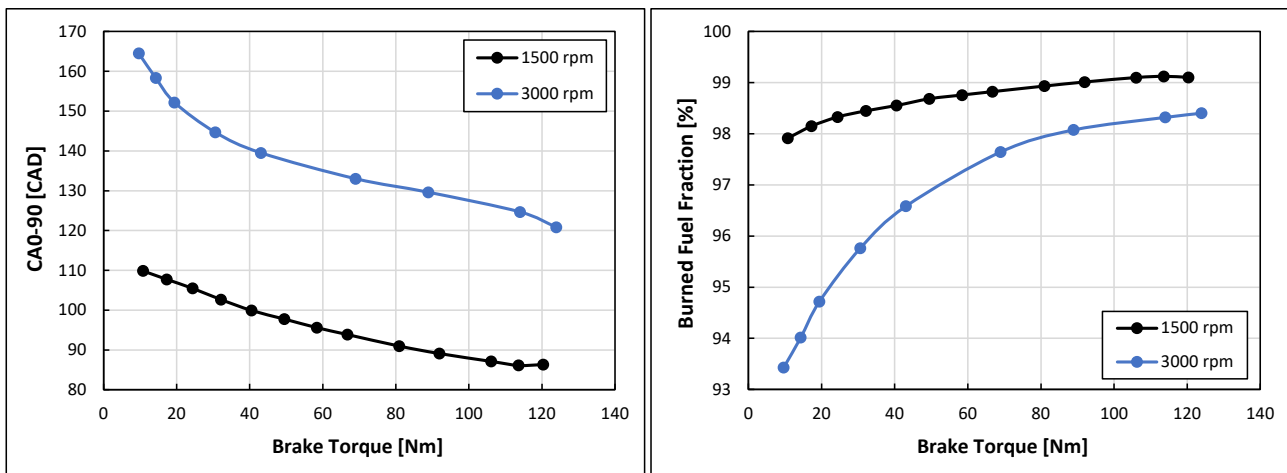


Figure 16. CA0-90 (left) and burned fuel fraction (right) vs. engine torque for both 1500 and 3000 rpm operating points. $\phi = 1$, no boost.

4. Conclusions

In this paper, the performance and the operating limits of a downsized PFI SI engine fueled with pure ammonia were estimated by means of a 1D predictive model. 3D calculations were performed to verify the reliability of the results provided by the 1D approach. The main results can be summarized as follows:

- The low laminar flame speed of ammonia–air mixtures leads to increased combustion durations and to optimal spark timings more advanced than typical ones of SI engines. On the other hand, no knock occurrence was detected.
- At 1500 rpm, no boost WOT condition and fixed spark advance, the ammonia burned fuel fraction decreases with decreasing equivalence ratios. Despite the maximum engine efficiency (38.6%) and the minimum BSFC (415 g/kWh) being reached for $\phi = 0.9$, both the lowest combustion duration and the minimum ammonia content in the exhaust gas are obtained for $\phi = 1$.
- Considering unthrottled engine operation and stoichiometric conditions, the combustion duration decreases for increasing boost pressure. Due to the operating limits of both in-cylinder pressure and exhaust gas temperature, the maximum regime which guarantees a proper engine operation is 3000 rpm, except for the highest boost level (BP = 1.8 bar).

- Imposing no boost WOT conditions and optimal spark timing, increasing compression ratios (from 9.8 to 11.0) lead to a reduction in the combustion duration (up to 11% at the maximum regime) and to a consequent increase in the burned fuel fraction (up to about 1.7% at the maximum regime). Of course, engine power slightly increases and BSFC decreases. The exhaust gas temperature also decreases, allowing the engine to properly operate at up to 4000 rpm.
- Considering no boost conditions, stoichiometric air–ammonia mixture and optimal spark timing, the more the engine is throttled, the more the burned fuel fraction decreases. This reduction increases with increasing speed (up to a burned fraction of about 93.5% at 3000 rpm), which can make it difficult to operate the engine at part load and medium engine speeds.
- Properly tuned, the ammonia engine shows really interesting efficiencies (up to about 41% at the maximum allowable BP). At a given engine speed, the delivered power is comparable to that of the same engine fueled with gasoline. Of course, limits on the maximum speed greatly reduce the specific power compared to that of conventional engines.

It is worth noting that the analysis was carried out using a predictive model that does not allow evaluation the engine operating stability. This could further reduce the operating ranges found.

In the end, ammonia could be a very interesting fuel due to the absence of carbon dioxide emissions and low storage and transport costs. However, this analysis clearly shows that pure ammonia could excessively limit the operating range of a light-duty spark-ignition engine. On the other hand, the results suggest that this fuel could be suitable to power engines characterized by low engine speeds and high geometrical compression ratios.

Author Contributions: Conceptualization, D.L. and E.G.; methodology, D.L., E.G. and G.D.; formal analysis, D.L., E.G. and G.D.; investigation, D.L. and G.D.; data curation, D.L. and G.D.; writing—original draft preparation, D.L., E.G. and G.D.; writing—review and editing, D.L., E.G., G.F. and G.D.; supervision, E.G. and G.F. All authors have read and agreed to the published version of the manuscript.

Funding: This research received no external funding.

Data Availability Statement: Not applicable.

Conflicts of Interest: The authors declare no conflict of interest.

Nomenclature

1D	One-dimensional
3D	Three-dimensional
aTDC	After top dead center
BDC	Bottom dead center
BP	Boost pressure
BSFC	Brake specific fuel consumption
bTDC	Before top dead center
CA0-2	0–2% mass fraction fuel burn duration
CA0-90	0–90% mass fraction fuel burn duration
CA10-90	10–90% mass fraction fuel burn duration
CAD	Crank angle degree
CI	Compression ignition
COV _{IMEP}	Coefficient of variation of IMEP
CR	Compression ratio
EVO	Exhaust valve opening
GDI	Gasoline direct injection
KI	Knock intensity
ICE	Internal combustion engine

IME	Indicated mean effective pressure
NO _x	Nitrogen oxides
PFI	Port fuel injection
SA	Spark advance
SI	Spark ignition
TDC	Top dead center
WOT	Wide open throttle
ϕ	Equivalence ratio

References

- Valera-Medina, A.; Xiao, H.; Owen-Jones, M.; David, W.; Bowen, P. Ammonia for power. *Prog. Energy Combust. Sci.* **2018**, *69*, 63–102. [[CrossRef](#)]
- Giddey, S.; Badwal, S.P.S.; Munnings, C.; Dolan, M. Ammonia as a Renewable Energy Transportation Media. *ACS Sustain. Chem. Eng.* **2017**, *5*, 10231–10239. [[CrossRef](#)]
- Cardoso, J.S.; Silva, V.; Rocha, R.C.; Hall, M.J.; Costa, M.; Eusébio, D. Ammonia as an energy vector: Current and future prospects for low-carbon fuel applications in internal combustion engines. *J. Clean. Prod.* **2021**, *296*, 126562. [[CrossRef](#)]
- Thurston, R.H. A History of the Growth of the Steam-Engine. *Nature* **1879**, *19*, 381–382. [[CrossRef](#)]
- Kobayashi, H.; Hayakawa, A.; Somarathne, K.K.A.; Okafor, E.C. Science and technology of ammonia combustion. *Proc. Combust. Inst.* **2019**, *37*, 109–133. [[CrossRef](#)]
- Mørch, C.; Bjerre, A.; Gøttrup, M.; Sorenson, S.; Schramm, J. Ammonia/hydrogen mixtures in an SI-engine: Engine performance and analysis of a proposed fuel system. *Fuel* **2011**, *90*, 854–864. [[CrossRef](#)]
- Onorati, A.; Payri, R.; Vaglieco, B.; Agarwal, A.; Bae, C.; Bruneaux, G.; Canakci, M.; Gavaises, M.; Günthner, M.; Hasse, C.; et al. The role of hydrogen for future internal combustion engines. *Int. J. Engine Res.* **2022**, *23*, 529–540. [[CrossRef](#)]
- Mounaïm-Rousselle, C.; Bréquigny, P.; Medina, A.V.; Boulet, E.; Emberson, D.; Løvås, T. Ammonia as Fuel for Transportation to Mitigate Zero Carbon Impact. In *Engines and Fuels for Future Transport*; Springer: Berlin/Heidelberg, Germany, 2021; pp. 257–279. [[CrossRef](#)]
- Hansson, J.; Brynolf, S.; Fridell, E.; Lehtveer, M. The Potential Role of Ammonia as Marine Fuel—Based on Energy Systems Modeling and Multi-Criteria Decision Analysis. *Sustainability* **2020**, *12*, 3265. [[CrossRef](#)]
- Rodríguez, C.G.; Lamas, M.I.; Rodríguez, J.D.D.; Abbas, A. Possibilities of Ammonia as Both Fuel and NO_x Reductant in Marine Engines: A Numerical Study. *J. Mar. Sci. Eng.* **2022**, *10*, 43. [[CrossRef](#)]
- Chiong, M.-C.; Chong, C.T.; Ng, J.-H.; Mashruk, S.; Chong, W.W.F.; Samiran, N.A.; Mong, G.R.; Valera-Medina, A. Advancements of combustion technologies in the ammonia-fuelled engines. *Energy Convers. Manag.* **2021**, *244*, 114460. [[CrossRef](#)]
- Xu, X.; Liu, E.; Zhu, N.; Liu, F.; Qian, F. Review of the Current Status of Ammonia-Blended Hydrogen Fuel Engine Development. *Energies* **2022**, *15*, 1023. [[CrossRef](#)]
- Grannell, S.M.; Assanis, D.N.; Bohac, S.V.; Gillespie, D.E. The Operating Features of a Stoichiometric, Ammonia and Gasoline Dual Fueled Spark Ignition Engine. In Proceedings of the ASME 2006 International Mechanical Engineering Congress and Exposition, Energy Conversion and Resources, Chicago, IL, USA, 5–10 November 2006; pp. 15–27. [[CrossRef](#)]
- Reiter, A.J.; Kong, S.-C. Combustion and emissions characteristics of compression-ignition engine using dual ammonia-diesel fuel. *Fuel* **2011**, *90*, 87–97. [[CrossRef](#)]
- Dimitriou, P.; Javaid, R. A review of ammonia as a compression ignition engine fuel. *Int. J. Hydrogen Energy* **2020**, *45*, 7098–7118. [[CrossRef](#)]
- Sun, X.; Liu, H.; Duan, X.; Guo, H.; Li, Y.; Qiao, J.; Liu, Q.; Liu, J. Effect of hydrogen enrichment on the flame propagation, emissions formation and energy balance of the natural gas spark ignition engine. *Fuel* **2021**, *307*, 121843. [[CrossRef](#)]
- Duan, X.; Liu, Y.; Liu, J.; Lai, M.-C.; Jansons, M.; Guo, G.; Zhang, S.; Tang, Q. Experimental and numerical investigation of the effects of low-pressure, high-pressure and internal EGR configurations on the performance, combustion and emission characteristics in a hydrogen-enriched heavy-duty lean-burn natural gas SI engine. *Energy Convers. Manag.* **2019**, *195*, 1319–1333. [[CrossRef](#)]
- Lhuillier, C.; Brequigny, P.; Contino, F.; Rousselle, C. Combustion Characteristics of Ammonia in a Modern Spark-Ignition Engine. In Proceedings of the Conference on Sustainable Mobility, Catane, Italy, 14–15 October 2019.
- Lhuillier, C.; Brequigny, P.; Contino, F.; Rousselle, C. Performance and Emissions of an Ammonia-Fueled SI Engine with Hydrogen Enrichment. In Proceedings of the 14th International Conference on Engines & Vehicles, Capri, Italy, 15–19 September 2019.
- Mounaïm-Rousselle, C.; Bréquigny, P.; Dumand, C.; Houillé, S. Operating Limits for Ammonia Fuel Spark-Ignition Engine. *Energies* **2021**, *14*, 4141. [[CrossRef](#)]
- Guo, B.; Ichiyanagi, M.; Kajiki, K.; Aratake, N.; Zheng, Q.; Kodaka, M.; Suzuki, T. Combustion Analysis of Ammonia Fueled High Compression Ratio SI Engine with Glow Plug and Sub-Chamber. *Int. J. Automot. Eng.* **2022**, *13*, 1–8. [[CrossRef](#)]
- Abd El Fattah, S.F.; Ezzat, M.F.; Mourad, M.A.; Elkelawy, M.; Youssef, I.M. Youssef Experimental Investigation of the Performance and Exhaust Emissions of a Spark-Ignition Engine Operating with Different Proportional Blends of Gasoline and Water Ammonia Solution. *J. Eng. Res.* **2021**, *5*, 38–45.

23. Şahin, Z.; Akcanca, I.Z.; Durgun, O. Experimental investigation of the effects of ammonia solution (NH₃OH) on engine performance and exhaust emissions of a small diesel engine. *Fuel* **2018**, *214*, 330–341. [[CrossRef](#)]
24. Lanni, D.; Galloni, E.; Fontana, G. Numerical analysis of the effects of port water injection in a downsized SI engine at partial and full load operation. *Appl. Therm. Eng.* **2022**, *205*, 118060. [[CrossRef](#)]
25. Galloni, E.; Lanni, D.; Fontana, G.; D'Antuono, G.; Stabile, S. Performance Estimation of a Downsized SI Engine Running with Hydrogen. *Energies* **2022**, *15*, 4744. [[CrossRef](#)]
26. Metghalchi, M.; Keck, J.C. Burning Velocities of Mixtures of air with Methanol, Isooctane, and Indolene at High Pressure and Temperature. *Combust. Flame* **1982**, *48*, 191–210. [[CrossRef](#)]
27. Metghalchi, M.; Keck, J.C. Laminar Burning Velocity of Propane-Air Mixtures at High Temperature and Pressure. *Combust. Flame* **1980**, *38*, 143–154. [[CrossRef](#)]
28. Bozza, F.; Fontana, G.; Galloni, E.; Torella, E. 3D-1D Analyses of the Turbulent Flow Field, Burning Speed and Knock Occurrence in a Turbocharged SI Engine. *SAE Trans. J. Engines* **2007**, *116*, 1495–1507.
29. Livengood, J.; Wu, P. Correlation of autoignition phenomena in internal combustion engines and rapid compression machines. *Symp. (International) Combust.* **1955**, *5*, 347–356. [[CrossRef](#)]
30. Richard, S.; Bougrine, S.; Font, G.; Lafossas, F.-A.; Le Berr, F. On the Reduction of a 3D CFD Combustion Model to Build a Physical 0D Model for Simulating Heat Release, Knock and Pollutants in SI Engines. *Oil Gas Sci. Technol.-Rev. IFP Energies Nouv.* **2009**, *64*, 223–242. [[CrossRef](#)]
31. Scala, F.; Galloni, E.; Fontana, G. Numerical analysis of a downsized spark-ignition engine fueled by butanol/gasoline blends at part-load operation. *Appl. Therm. Eng.* **2016**, *102*, 383–390. [[CrossRef](#)]
32. Goldmann, A.; Dinkelacker, F. Approximation of laminar flame characteristics on premixed ammonia/hydrogen/nitrogen/air mixtures at elevated temperatures and pressures. *Fuel* **2018**, *224*, 366–378. [[CrossRef](#)]
33. Heywood, J.B. *Internal Combustion Engine Fundamentals*; McGraw-Hill: New York, NY, USA, 2018.
34. Chen, J.; Jiang, X.; Qin, X.; Huang, Z. Effect of hydrogen blending on the high temperature auto-ignition of ammonia at elevated pressure. *Fuel* **2020**, *287*, 119563. [[CrossRef](#)]
35. Nakamura, H.; Hasegawa, S.; Tezuka, T. Kinetic modeling of ammonia/air weak flames in a micro flow reactor with a controlled temperature profile. *Combust. Flame* **2017**, *185*, 16–27. [[CrossRef](#)]